

RSC Advances



This is an *Accepted Manuscript*, which has been through the Royal Society of Chemistry peer review process and has been accepted for publication.

Accepted Manuscripts are published online shortly after acceptance, before technical editing, formatting and proof reading. Using this free service, authors can make their results available to the community, in citable form, before we publish the edited article. This *Accepted Manuscript* will be replaced by the edited, formatted and paginated article as soon as this is available.

You can find more information about *Accepted Manuscripts* in the [Information for Authors](#).

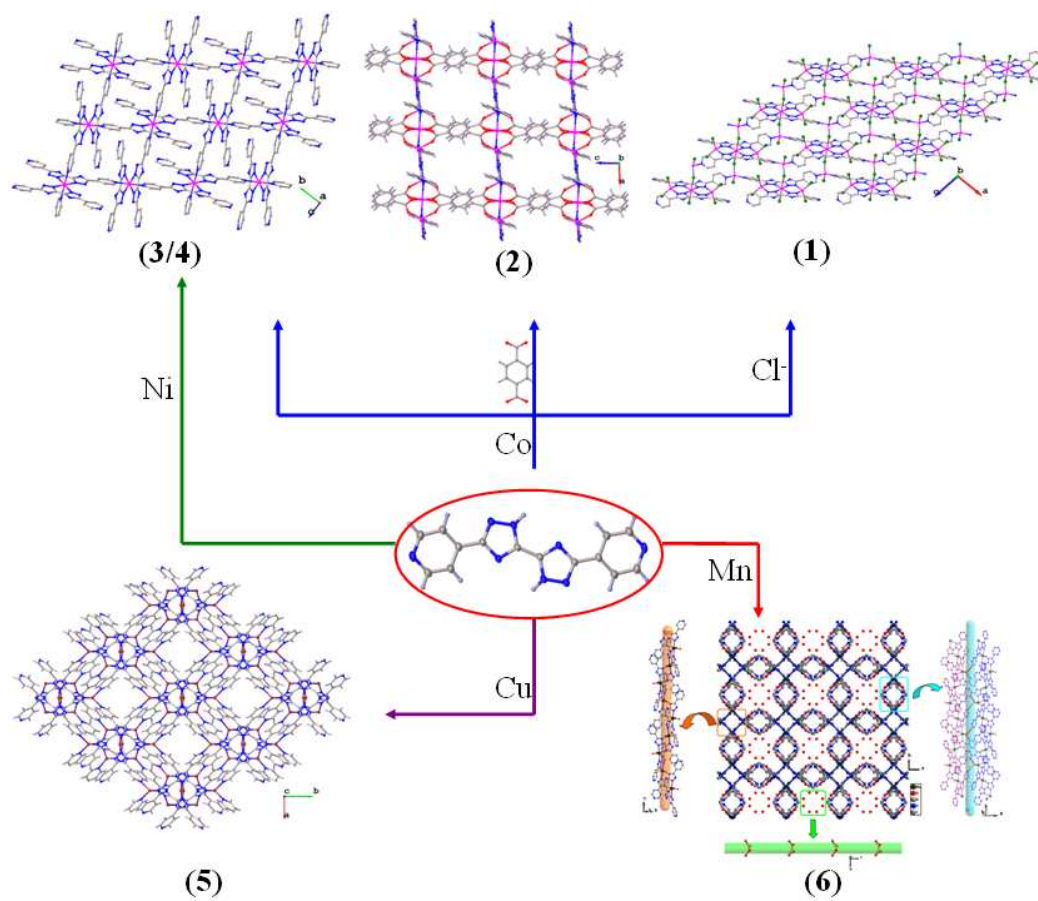
Please note that technical editing may introduce minor changes to the text and/or graphics, which may alter content. The journal's standard [Terms & Conditions](#) and the [Ethical guidelines](#) still apply. In no event shall the Royal Society of Chemistry be held responsible for any errors or omissions in this *Accepted Manuscript* or any consequences arising from the use of any information it contains.

A Series of Multidimensional MOFs Incorporating a new N-heterocyclic Building Block:

5,5'-di(pyridin-4-yl)-3,3'-bi(1,2,4-triazole)

Peng-Fei Yao,^a Hai-Ye Li,^a Fu-Ping Huang,* Qing Yu,^a Xiao-Huan Qin,^a Jie Tang,^a Ye Tao,^a He-Dong Bian*^b

By using a new N-heterocyclic Building Block: 5,5'-di(pyridin-4-yl)-3,3'-bi(1,2,4-triazole) (4,4'-H₂dbpt), six novel coordination polymers with diversiform connectivity from one to three dimensional were constructed and characterized by X-ray crystallography successfully. Additionally, the magnetic properties of **1-4** have been briefly investigated.



A Series of Multidimensional MOFs Incorporating a new N-heterocyclic Building Block:

5,5'-di(pyridin-4-yl)-3,3'-bi(1,2,4-triazole)

Peng-Fei Yao,^a Hai-Ye Li,^a Fu-Ping Huang,^{*a} Qing Yu,^a Xiao-Huan Qin,^a Jie Tang,^a
Ye Tao^a, He-Dong Bian^{*b}

ABSTRACT: By using a new N-heterocyclic Building Block: 5,5'-di(pyridin-4-yl)-3,3'-bi(1,2,4-triazole) (4,4'- H₂dbpt), six novel coordination polymers with diversiform connectivity from one to three dimensional were constructed successfully. By regulating the different auxiliary ligands, central metal ions, and some other synthetic conditions, 4,4'- H₂dbpt revised various coordination modes. Consequently, **1** revise a 2D (3, 6)-topology, with (4³)₃(4⁶.6⁶.8³)₂ Schläfli symbol. **2** show a 3D 8- connected topology with (3⁶.4¹⁸.5³.6) Schläfli symbol. **3** and **4** which are isostructural, both have a 2D 4- connected topology, with (4⁴.6²) Schläfli symbol. **5** have a complex 3D porous architecture with a 1D solvent-filled channel. **6** reveal a 1D helical chain extended along a quad screw axis. These results indicate that 4,4'- H₂dbpt is an excellent multi- connection linker to construct MOFs with interesting structures and properties.

Introduction

The design and synthesis of coordination polymers, especially metal– organic frameworks (MOFs) have attracted considerable interest in the realm of supra-

^{*a} Key Laboratory for the Chemistry and Molecular Engineering of Medicinal Resources (Ministry of Education of China), School of Chemistry and Pharmacy, Guangxi Normal University, Guilin, 541004, P. R. China. E-mail: huangfp2010@163.com

^{*b} School of Chemistry and Chemical Engineering, Guangxi University for Nationalities, Key Laboratory of Chemistry and Engineering of Forest Products, Nanning, 530008, P. R. China. E-mail: gxunchem@163.com

molecular chemistry and crystal engineering, not only owing to their appealing structural and topological novelty but also because of their tremendous potential applications in gas storage and separation,[1] electrical conduction,[2] luminescence materials,[3] molecular magnets, [4] and heterogeneous catalysis.[5] Thus, a series of studies in this field have mainly focused on the design and preparation, as well as the structure–property relationships.[6] The structures of coordination polymers are determined by several factors, including the coordination geometry of the central metal ions, solvents,[7] ligand structure, metal-ligand ratio,[8] counterions,[9] pH,[10] temperature,[11] and so on. Among the reported studies, much effort has been focused on the rational design and controlled synthesis of coordination polymers using multidentate ligands such as polycarboxylate and N- heterocyclic ligands. The N-heterocyclic ligands are good molecular building blocks and co- ligands for constructing MOFs with interesting structures and properties, which have been widely reported by Yaghi,[12] Snurr,[13] Chen,[14] Du,[15] Tong,[16] Zhang,[17] etc.

Our groups have systematically explored the coordination assemblies on the basis of some polycarboxylate ligands cooperate with some angular N-heterocyclic-like ligands:

1H-3,5-bis(4-pyridyl)-1,2,4-triazole	(4,4'-bpt),
1H-3-(3-pyridyl)-5-(4-pyridyl)-1,2,4-triazole	(3,4'-bpt),
1H-3,5-bis(3-pyridyl)-1,2,4-triazole	(3,3'-bpt),
4- amino-3,5-bis(4-pyridyl)-1,2,4-triazole	(4,4'-abpt),

1,4-bis(5-(4-pyridyl)-1H-1,2,4-triazol-3-yl)benzene (bptb), etc. [18] In most of the cases, the angular N-heterocyclic-like ligands act as 2- connected linkers with different distortion angles and directions. Relying on the versatile coordination modes of the polycarboxylate ligands, a variety of structures were obtained. Recently, various compounds with complex topology based on some ditriazole- pyridine ligand, have been reported by Hou,[19] Li,[20] Sha,[21] and Zhou,[22] etc. And these ligands revised various conformations, highlighting they are another excellent multi-connection linkers in addition to polycarboxylate ligands.[23] Thus, these considerations inspired us to explore new coordination frameworks with this kind of ligands.

In this paper, we introduce a new ditriazole-pyridine ligand: 5,5'-di(pyridin-4-yl)-3,3'-bi(1,2,4-triazole) (4,4'-H₂dbpt). Different with our previous N-heterocyclic-like ligands, chelate effect between the adjacent triazole rings was introduced. Thus, it could adopt various conformations, which may lead to unpredictable and interesting structures, by regulating the rotation angles of the four aromatic rings with respect to each other, the deprotonation effect (4,4'-H₂dbpt, 4,4'-Hdbpt⁻, 4,4'-dbpt²⁻) and the flexing angles. However, to the best of our knowledge, MOFs based on 5,5'-di(pyridin-4-yl)-3,3'-bi(1,2,4-triazole) (4,4'-H₂dbpt) have never been documented to date.

A series of coordination polymers based on 4,4'-H₂dbpt, namely, {[Co₅(4,4'-dbpt)₂Cl₈]•2(C₂H₅)₃NH}_n (**1**), {[Co₃(*p*-BDC)₂(4,4'-dbpt)•0.5CH₃OH]}_n (**2**), {[Co(4,4'-Hdbpt)₂]•H₂O}_n (**3**), {[Ni(4,4'-Hdbpt)₂]•H₂O}_n (**4**), {[Cu₂(4,4'-dbpt)•H₂O}_n (**5**), {[Mn(4,4'-dbpt)(H₂O)₂]•2H₂O}_n (**6**) were constructed successfully. By regulating the different auxiliary ligands, central metal ions, etc, 4,4'-H₂dbpt revised five different coordination modes (scheme 1) based on the alteration of the rotation angles, valence state and the flexing angles. As a result, **1-6** revised five different (**3** and **4** are isostructural) architectures with diversiform connectivity from one to three dimensional.

Scheme 1

Experimental Section

Materials and Physical Measurements

With the exception of the ligand of 4,4'-H₂dbpt which was prepared according to the literature procedure,[24] all reagents and solvents for synthesis and analysis were commercially available and used as received. IR spectra were taken on a Perkin-Elmer spectrum One FT-IR spectrometer in the 4000-400 cm⁻¹ region with KBr pellets. Elemental analyses for C, H and N were carried out on a Model 2400 II, Perkin-Elmer elemental analyzer. The magnetic susceptibility measurements of the polycrystalline

samples were measured over the temperature range of 2- 300K with a Quantum Design MPMS-XL7 SQUID magnetometer using an applied magnetic field of 1000 Oe. A diamagnetic correction to the observed susceptibilities was applied using Pascal's constants. X-ray powder diffraction (XRPD) intensities were measured on a Rigaku D/max-III A diffractometer ($Cu-K\alpha$, $\lambda = 1.54056 \text{ \AA}$). The single crystalline powder samples were prepared by crushing the crystals and scanned from 3 to 60° with a step of $0.1^\circ/s$. Calculated patterns of **1- 6** were generated with PowderCell.

Syntheses of complexes **1– 6**

{[Co₅(4,4'-dbpt)₂Cl₈]• 2(C₂H₅)₃NH}_n (1). A mixture containing 4,4'- H₂dbpt (87 mg, 0.3mmol), CoCl₂•6H₂O (238 mg, 1 mmol), ethanol (15 mL) and triethylamine (0.5 mL) was sealed in a Teflon-lined stainless steel vessel (25 mL), which was heated at 160 °C for 3 days and then cooled to room temperature at a rate of 10 °C/h. Glaucous needle-like crystals of **1** were obtained and picked out, washed with ethanol and dried in air. Yield: 47% (based on Co(II)). Elemental analysis for C₄₀H₄₆Cl₈Co₅N₁₈ (%) Calcd: C, 35.40; H, 3.42; N, 18.58. Found: C, 35.47; H, 3.49; N, 18.52. IR (KBr, cm⁻¹): 3410s, 1620s, 1437s, 1354m, 1307s, 1217w, 1160w, 1066m, 1019s, 839s, 713s, 616w, 576s, 526, 436.

{[Co₃(*p*-BDC)₂(4,4'-dbpt)• 0.5CH₃OH]}_n (2). A mixture containing 4,4'- H₂dbpt (87 mg, 0.3mmol), Co(NO₃)₂•6H₂O (291 mg, 1 mmol), *p*- H₂BDC (83 mg, 0.5 mmol), water (10 mL), methanol (5 mL) and triethylamine (0.5 mL) was sealed in a Teflon-lined stainless steel vessel (25 mL), which was heated at 160 °C for 3 days and then cooled to room temperature at a rate of 10 °C/h. Purple block crystals of **2** were obtained and picked out, washed with distilled water and dried in air. Yield: 30% (based on Co(II)). Anal. Calcd for (C_{30.5}H₁₈Co₃N₈O_{8.5}): C, 45.26; H, 2.24; N, 13.85. Found: C, 45.39; H, 2.17; N, 13.92. IR (KBr, cm⁻¹): 3446s, 1717m, 1599s, 1498w, 1426m, 1365s, 1300m, 1271m, 1217w, 1156w, 1102w, 1016m, 882w, 839m, 814s, 742s, 717m, 587m, 515w, 450w.

{[Co(4,4'-Hdbpt)₂]• 2H₂O}_n (3). A mixture containing 4,4'- H₂dbpt (87 mg, 0.3mmol), Co(NO₃)₂•6H₂O (291 mg, 1 mmol), water (15 mL), and triethylamine (0.5

mL) was sealed in a Teflon-lined stainless steel vessel (25 mL), which was heated at 160 °C for 3 days and then cooled to room temperature at a rate of 10 °C/h. Orange block X-ray-quality crystals of **3** in a 32% yield (based on Co (II)). Anal. Calcd for (C₂₈H₂₂CoN₁₆O₂): C, 49.93; H, 3.29; N, 33.27. Found: C, 49.81; H, 3.35; N, 33.18. IR (KBr, cm⁻¹): 3428s, 3028m, 2668m, 1620s, 1574m, 1559w, 1426s, 1390m, 1329w, 1304s, 1210m, 1178s, 1113m, 1052m, 1008s, 990s, 890m, 961w, 839s, 753w, 724s, 699m, 656w, 533m, 515s, 461w, 418w.

{[Ni(4,4'-Hdbpt)₂]• 2H₂O}_n (**4**). The same synthetic procedure as that for **3** was used except that Co(NO₃)₂•6H₂O was replaced by Ni(NO₃)₂•6H₂O giving green needle-like X-ray-quality crystals of **4** in a 39% yield (based on Ni (II)). Anal. Calcd for (C₂₈H₂₂NiN₁₆O₂): C, 49.95; H, 3.29; N, 33.29. Found: C, 49.86; H, 3.31; N, 33.15. IR (KBr, cm⁻¹): 3428s, 3028m, 2668m, 1620s, 1574m, 1559w, 1307s, 1214m, 1174s, 1113m, 1052m, 1012m, 990s, 980m, 890w, 861m, 839s, 756s, 724s, 699m, 652w, 533m, 515s, 461w, 422w.

{[Cu₂(4,4'-dbpt)]• H₂O}_n (**5**). The same synthetic procedure as that for **3** was used except that Co(NO₃)₂•6H₂O and water were replaced by Cu(NO₃)₂•6H₂O and DMF, respectively, giving red needle-like X-ray-quality crystals of **5** in a 45% yield (based on Cu(I)). Anal. Calcd for (C₁₄H₁₀Cu₂N₈O): C, 38.80; H, 2.33; N, 25.86. Found: C, 38.87; H, 2.29; N, 25.93. IR (KBr, cm⁻¹): 3435s, 3107w, 3050w, 2456w, 1944w, 1660w, 1610s, 1516m, 1430s, 1383m, 1318s, 1214w, 1152w, 1098w, 1030w, 1005m, 987m, 839s, 746w, 710s, 526w, 497w.

{[Mn(4,4'-dbpt)(H₂O)₂]• 2H₂O}_n (**6**). The same synthetic procedure as that for **3** was used except that Co(NO₃)₂•6H₂O was replaced by Mn(NO₃)₂•6H₂O giving colourless needle-like X-ray-quality crystals of **6** in a 44% yield (based on Mn(II)). Anal. Calcd for (C₁₄H₁₆MnN₈O₄): C, 40.49; H, 3.88; N, 26.98. Found: C, 40.57; H, 3.72; N, 27.07. IR (KBr, cm⁻¹): 3415s, 3046w, 2948w, 1932w, 1612s, 1526w, 1499m, 1455w, 1434s, 1403m, 1385w, 1351w, 1317s, 1292m, 1234w, 1215w, 1157w, 1120w, 1092w, 1065w, 1006s, 834m, 745w, 723m, 708s, 671w, 640w, 523w, 489w.

X-ray Crystallographic Determination

All reflection data were collected on an Agilent Supernova diffractometer (Mo, $\lambda = 0.71073\text{\AA}$) at room temperature. A semiempirical absorption correction by using the SADABS program was applied, and the raw data frame integration was performed with SAINT[25]. The crystal structures were solved by the direct method using the program SHELXS-97[26] and refined by the full-matrix least-squares method on F^2 for all non-hydrogen atoms using SHELXL-97[27] with anisotropic thermal parameters. All hydrogen atoms were located in calculated positions and refined isotropically, except the hydrogen atoms of water molecules were fixed in a difference Fourier map and refined isotropically. The details of the crystal data were summarized in Table 1, and selected bond lengths and angles for compounds **1–6** are listed in Table S1. The crystallographic data of **1–6** in CIF format has been deposited in the Cambridge Crystallographic Data Center (CCDC reference number: 1033515-1033520).

XRPD Results

To confirm whether the crystal structures are truly representative of the bulk materials, X-ray powder diffraction (XRPD) experiments have also been carried out for **1–6**. The XRPD experimental and computer-simulated patterns of the corresponding complexes are shown in ESI, Figure S2. Although the experimental patterns have a few unindexed diffraction lines and some are slightly broadened in comparison with those simulated from the single crystal models, it can still be considered favorably that the bulk synthesized materials and the as-grown crystals are homogeneous for **1–6**.

Results and discussion

Description of the crystal structures

Table 1

$\{[\text{Co}_5(4,4'\text{-dbpt})_2\text{Cl}_3] \cdot 2(\text{C}_2\text{H}_5)_3\text{NH}\}_n$ (**1**). Single crystal X-ray diffraction analysis reveals that the asymmetric unit of **1** contains three crystallographically independent Co atoms, one 4,4'-dbpt²⁻ anionic, four Cl⁻ anionic, and one lattice protonated triethylamine ion. As illustrated in Fig. 1a, Co1 is coordinated by two N atoms (N6, N3A, symmetry codes: A: $x, y, z+1$) from two 4,4'-dbpt ligands, and two Cl atoms (Cl1, Cl2), to yield distorted tetrahedron geometry. Co3 also adopts a distorted tetrahedron geometry coordinated by two N atoms (N1C, N8D, C: $-x+1, -y+1, -z+1$; D: $x, y, z-1$) from two 4,4'-dbpt ligands, one μ_2 -Cl (Cl3) atom and one terminal Cl atom (Cl4). While Co2 lying on a symmetry center adopts a distorted octahedron geometry coordinated by four N atoms (N4, N5, N4A, N5A) from two 4,4'-dbpt ligands in the equatorial plane, and two μ_2 -Cl atoms (Cl3, Cl3A) in the axial position. The middle Co2 ion is linked to terminal Co1 and Co3 ions with two triazoles from two 4,4'-dbpt ligands (Co1...Co2= 3.788 (2) Å) and one μ_2 -Cl⁻ (Co2...Co3= 4.493 (2) Å) respectively to form a Co₅ unit (Fig. 1b). The adjacent Co₅ units share vertices (Co3) and connect each other, to form a 2D ladder structure (Fig. 1c). The lattice protonated triethylamine ions fill in the gaps of the neighbor 2D layers which arrange parallelly each other (Fig. 1d). A topological analysis reveals that the Co₅ unit and the shared vertices Co3 serve as a 6-connected node and 3-connected node respectively to link each other. According to Wells' topology definition,^[28] an interesting topology with the short Schläfli symbol of $(4^3)_3(4^6 \cdot 6^6 \cdot 8^3)_2$ is formed (Fig. 1e).

Fig. 1

$\{[\text{Co}_3(p\text{-BDC})_2(4,4'\text{-dbpt}) \cdot 0.5\text{CH}_3\text{OH}]\}_n$ (**2**). The asymmetric unit of **2** contains two crystallographically independent Co atoms, half a 4,4'-dbpt²⁻, one *p*-BDC anionic, and a quarter lattice methanol molecule. As illustrated in Fig. 2, **2** reveals a novel 3D coordination polymer with a linear trinuclear Co(II) unit. In the trinuclear unit, the

middle Co1 ions lying on a symmetry center exhibit a distorted octahedron geometry coordinated by four O atoms (O1, O3, O1A, O3A, A: $-x+1, -y+1, -z+1$) from four *p*-BDC ligands in the equatorial plane, and two N atoms (N3B, N3C, B: $-x, -y+1, -z+1$; C: $x+1, y, z$) from two dbpt ligands in the axial position. The terminal Co2 ions exhibit a distorted trigonal- bipyramidal geometry, which is provided by surround by two N atoms (N2C, N4D, D: $-x, -y, -z+1$) from two 4,4'- dbpt ligands in the axial position, two O atoms (O2A, O4A) from two *p*-BDC ligands and one N atom (N4D, D: $-x, -y, -z+1$) from 4,4'- dbpt ligand in the equatorial plane. The middle Co1 ion is linked to terminal Co2 ions with two syn- syn carboxylate from two *p*-BDC ligands and a triazole from 4,4'- dbpt [$\text{Co}^{\cdots} \text{Co} = 4.008 (5) \text{ \AA}$] to form the Co_3 unit. The adjacent Co_3 units are connected by 4,4'- dbpt²⁻ with mode 2 (Scheme 1) to form a 2D layer (Fig. 2b). The layer is further connected by *p*-BDC pillars to generate a 3D open framework with a 1D solvent-filled channel which diameter is about 9 Å (Fig. 2d). Better insight into this framework can be achieved by topology analysis. The Co_3 unit serves as an 8- connected node, *p*-BDC and 4,4'- dbpt both serves as linker. In this way, this framework can be simplified to be an 8 -connected 3D architecture with the short Schläfli symbol of $(3^6.4^{18}.5^3.6)$ is formed (Fig. 2e).

Fig. 2

$\{[\text{M}(4,4'\text{-dbpt})_2] \cdot 2\text{H}_2\text{O}\}_n$ (M= Co for **3**, Ni for **4**). Compounds **3** and **4** are isostructural with an identical space group and similar cell dimensions. As shown in Fig. 3a, there is only one independent M atom in the asymmetric unit. All the M ions lying on a symmetry center exhibit a distorted octahedron geometry coordinated by four triazole N atoms (N4, N5, N4B, N5B, B: $x+1/2, -y-1/2, z-1/2$) from two 4,4'- Hdbpt⁻ ions in the equatorial plane, and two pyridine N atoms (N8A, N8C, A: $-x+1, -y, -z+2$; C: $-x+1/2, y+1/2, -z+5/2$) from two 4,4'- Hdbpt⁻ ions in the axial position. The adjacent M ions are connected by 4,4'- Hdbpt⁻ with mode 3 (Scheme 1) with the separation of 10.56 (1) Å for **3** and 10.54 (1) Å for **4**, to form a 2D layer (Fig. 2b). And the neighbor 2D layers arrange parallelly each other (Fig. 3c). The distance of the

nearest M atoms between the neighbor 2D layers is 9.25 (1) Å for **3**, and 9.18 (1) Å for **4**. The M ion serves as a 4- connected node, and 4,4'- Hdbpt²⁻ serves as a linker. As a result, this framework can be simplified to be a 4 -connected 2D architecture with the short Schläfli symbol of (4⁴.6²) is formed (Fig. 3d).

Fig. 3

{[Cu₂(4,4'-dbpt)]• H₂O}_n (5). The asymmetric unit of **5** contains three crystallographically independent Cu atoms, one 4,4'- dbpt²⁻, and a lattice water molecule. As illustrated in Fig. 4a, Cu1 is coordinated by four N atoms (N1, N1A, N7B, N6C, Symmetry codes: A: $-x, y, -z+1/2$; B: $-x+1/2, y-1/2, z$; C: $x-1/2, y-1/2, -z+1/2$) from four 4,4'- dbpt ligands, to yield distorted tetrahedron geometry. Cu2 lying on a symmetry site is two- coordinated, which is provided by two triazole N donors (N4, N4D, D: $-x+1, y, -z+3/2$; (v) $x, -y+1, z+1/2$) from two 4,4'- dbpt ligands. The distance of Cu2- N5 is 2.913 (2) Å, indicating a weak coordination interaction between them. Cu3 adopt plane triangle configuration which is coordinated by three N atoms (N3, N6E, N8F, E: $x, -y+1, z+1/2$; F: $x-1/2, y-1/2, -z+3/2$) from three 4,4'- dbpt ligands. The 4,4'- dbpt ligand adopt mode 4 (Scheme 1) connect Cu(I) atoms to form a 3D reticular structure with a 1D solvent-filled channel which diameter is about 7 Å (Fig. 4b, c).

Fig. 4

{[Mn(4,4'-dbpt)(H₂O)₂]• 2H₂O}_n (6). Compound **6** crystallizes in the tetragonal space group *I4₁/acd*. As shown in Fig. 5a, there is only one independent Mn atom in the asymmetric unit. All the Mn atoms exhibit a distorted octahedron geometry coordinated by four triazole N atoms (N1, N1A, N3B, N3C, Symmetry codes: A: $-x+1/2, y, -z$; B: $-y+1/4, -x+1/4, -z+1/4$; C: $y+1/4, -x+1/4, z-1/4$) from two 4,4'- dbpt ligands, and two water molecules (O1, O1A). The adjacent Mn atoms are connected by 4,4'- dbpt²⁻ with mode 5 (Scheme 1) with the separation of 5.9493 (9) Å to form a quadruple helical chain extended along the *c* axis (Fig. 5b). The neighbor

helical chains arrange parallelly with the opposite spiral direction and connected each other through H-bond around another quad screw axis to form a 3D open framework with a 1D water-filled channel (Fig. 5c, d). And the water molecules in the channel arranged with S_4 symmetry (Fig. 5e). The distance of the nearest Mn atoms between the neighbor helical chains is 9.327 (1) Å.

Fig. 5

Structural Diversity of 1–6

Six new MOFs from one to three dimensions, based on the 4,4'-H₂dbpt ligand were presented. Among them, **1**, **3**, **4** form 2D layer architectures, **2** and **5** form 3D network architectures, and **6** forms 1D chain architecture with diversiform connectivity. Clearly, the phenomenon of structural diversification in **1–6** may arise from the three sources as follow. First of all, the 4,4'-H₂dbpt ligand plays a dominating effect on constructing the polymer structures. Owing to the different rotation angles of the four aromatic rings with respect to each other, deprotonation effect (4,4'-H₂dpbt, 4,4'-Hdpbt⁻, 4,4'-dpbt²⁻) and the flexing angles, it could adopt various conformations, which may lead to unpredictable and interesting structures. In this paper, the 4,4'-H₂dbpt ligand adopts five different conformations (Scheme 1) according to the geometric requirements of metal ions and/or the introduction of auxiliary ligand. Secondly, the introduction of auxiliary ligands may play significant roles in the formation of different topological structures. Compound **3** without auxiliary ligand, revealed a 2D 4- connected topology, with (4⁴.6²) Schläfli symbol. For **1**, Cl⁻ is involved in coordination. As a result, a more complex 2D ladder structure based on a Co₅ unit with the short Schläfli symbol of (4³)₃(4⁶.6⁶.8³)₂ is formed. For **2**, with the employment of H₂p-BDC, an 8- connected 3D pillared layered architecture with the short Schläfli symbol of (3⁶.4¹⁸.5³.6) is formed. Thirdly, different metal ions may have different charges, electron configurations, and ionic radii, hence exhibiting different

coordination geometries. So the connectivity of polymeric frameworks is also strongly related to the metal centers. In **5**, Cu(I) exhibit the coexistence of two, three and four-coordinated patterns which is different from others. And hence, a complex 3D architecture is formed.

Magnetic Properties

Magnetic susceptibility measurements were carried out on polycrystalline samples of **1-4** and **6** in the temperature range 2.0–300.0 K at 1000 Oe. (Fig 6a and 7)

For **1**, the data above 50 K follow the Curie–Weiss law with $C = 10.81 \text{ cm}^3\text{Kmol}^{-1}$ and $\theta = -22.35 \text{ K}$. The $\chi_M T$ value at 300 K is $10.12 \text{ cm}^3\cdot\text{K}\cdot\text{mol}^{-1}$, which is larger than the spin-only value $9.38 \text{ emu}\cdot\text{K}\cdot\text{mol}^{-1}$ for five magnetically active Co(II) ions ($S = 3/2$, $g = 2.0$), as expected for Co(II) systems with a significant contribution from the effects of spin-orbital coupling. As the temperature is lowered, the $\chi_M T$ values decrease continuously and reaches a local minimum of $5.98 \text{ cm}^3\cdot\text{K}\cdot\text{mol}^{-1}$ at about 12 K, indicative of a strong single-ion behavior admixture with a weak antiferromagnetic interaction [29]. And then increases slightly to reach a maximum at ca. 8.0 K, and then rapidly decreases to a minimum of $2.29 \text{ cm}^3\cdot\text{K}\cdot\text{mol}^{-1}$ at 2 K. The observed increase in $\chi_M T$ below this temperature is no longer coming from the single-ion behaviour but rather from a ferromagnetic or canted antiferromagnetic Co(II)–Co(II) exchange interaction, and the finally decreases in $\chi_M T$ below 10 K, indicating a magnetic phase transition. The dependence of $\chi_M T$ vs. T curves of **1** at different fields is pronounced at low-temperature, the larger increase of $\chi_M T$ values at a small field (Figure 6b). This is an important feature of spin-canting behavior.[30]

The zero-field ac susceptibility data of **1** shows obvious peaks and slight frequency-dependence (Fig. 6d, inset) below 8 K, which confirms the magnetic phase transition. And the shift of peak temperature (T_p) of χ_M'' for **1** was measured by a parameter $\phi = \Delta T_p / [T_p \Delta(\log f)] \approx 0.06$, being in the range of spin glass systems.[31] And the relaxation time τ_0 was obtained from the Arrhenius law; the best set of parameters is $\tau_0 = 2.53 \times 10^{-18} \text{ s}$ and $\Delta E/k_B = 201.55 \text{ K}$ (Fig 6d), where ΔE is the energy

barrier and k_B is the Boltzmann constant, suggesting a thermally activated mechanism.

Fig. 6

For **2**, the data above 2 K follow the Curie–Weiss law with $C = 7.48 \text{ cm}^3 \cdot \text{K} \cdot \text{mol}^{-1}$ and $\theta = -18.35 \text{ K}$. The $\chi_M T$ value at 300 K is $7.05 \text{ cm}^3 \cdot \text{K} \cdot \text{mol}^{-1}$, which is larger than the spin-only value $5.63 \text{ cm}^3 \cdot \text{K} \cdot \text{mol}^{-1}$ for three magnetically active Co(II) ions ($S = 3/2$, $g = 2.0$), as expected for Co(II) systems with a significant contribution from the effects of spin-orbital coupling. As the temperature is lowered, the $\chi_M T$ values decrease continuously and reaches a local minimum of $1.01 \text{ cm}^3 \cdot \text{K} \cdot \text{mol}^{-1}$ at about 2 K, indicative of a strong single-ion behavior admixture with a weak antiferromagnetic interaction.

For **3**, the data above 2 K follow the Curie–Weiss law with $C = 3.01 \text{ cm}^3 \cdot \text{K} \cdot \text{mol}^{-1}$ and $\theta = -12.47 \text{ K}$. The $\chi_M T$ value at 300 K is $2.89 \text{ cm}^3 \cdot \text{K} \cdot \text{mol}^{-1}$, which is much larger than the spin-only value $1.88 \text{ cm}^3 \cdot \text{K} \cdot \text{mol}^{-1}$ for a magnetically active Co(II) ion ($S = 3/2$, $g = 2.0$), as expected for Co(II) systems with a significant contribution from the effects of spin-orbital coupling. As the temperature is lowered, the $\chi_M T$ values decrease continuously and reaches a local minimum of $0.61 \text{ cm}^3 \cdot \text{K} \cdot \text{mol}^{-1}$ at about 2 K, indicative of a strong single-ion behavior. The distance of the nearest Co atoms in **3** is $9.25(1) \text{ \AA}$, indicating that the weak interactions between them could be ignored. The in- and out-of-phase ac susceptibilities have no dependence on frequency between 2 and 10 K for **3** indicating that there is no single-ion magnet (SIM) behavior in **3**. (Fig S3)

For **4**, the data above 2 K follow the Curie–Weiss law with $C = 1.33 \text{ cm}^3 \cdot \text{K} \cdot \text{mol}^{-1}$ and $\theta = -1.94 \text{ K}$. The $\chi_M T$ value at 300 K is $1.32 \text{ cm}^3 \cdot \text{K} \cdot \text{mol}^{-1}$, which is slightly larger than the spin-only value $1.21 \text{ cm}^3 \cdot \text{K} \cdot \text{mol}^{-1}$ for a magnetically active Ni(II) ion ($S = 1$, $g = 2.2$), and is relatively constant down to approximately 40 K. Below this temperature, it collapses, indicating significant ZFS in the $S = 1$ ground state. [32]

Similar to **3**, the distance of the nearest Ni atoms in **4** is 9.18 (1) Å, indicating that the weak interactions between them could be ignored. The in- and out-of-phase ac susceptibilities have no dependence on frequency between 2 and 10 K for **4** indicating that there is no SIM behavior in **4**. (Fig S3)

For **6**, the data above 2 K follow the Curie–Weiss law with $C = 4.73 \text{ cm}^3 \cdot \text{K} \cdot \text{mol}^{-1}$ and $\theta = -4.70 \text{ K}$. The χ_{MT} value at 300 K is $4.65 \text{ cm}^3 \cdot \text{K} \cdot \text{mol}^{-1}$, which is slightly larger than the spin-only value $4.38 \text{ cm}^3 \cdot \text{K} \cdot \text{mol}^{-1}$ for a magnetically active Mn(II) ion ($S = 5/2$, $g = 2.2$), and is relatively constant down to approximately 30 K. Below this temperature, the χ_{MT} values decrease continuously and reaches a local minimum of $1.27 \text{ cm}^3 \cdot \text{K} \cdot \text{mol}^{-1}$ at about 2 K, indicative of a weak antiferromagnetic Mn(II)–Mn(II) exchange interaction. The in- and out-of-phase ac susceptibilities have no dependence on frequency between 2 and 10 K. (Fig S3)

Fig. 7

Thermal Analyses

The thermogravimetric (TG) analysis was performed in N₂ atmosphere on polycrystalline samples of complex **1–6**, and the TG curves are shown in Fig. 8.

Fig. 8

For **1**, the first weight loss of 15.08% between 30 and 112 °C corresponds to the release of the lattice triethylamine molecules (calculated, 14.89%). The residual framework decomposed beyond 360 °C in a series of complicated weight losses until 920 °C. For **2**, the first weight loss of 1.82% between 30 and 85 °C

corresponds to the release of the lattice methyl alcohol molecules (calculated, 1.98%). The residual framework decomposed beyond 316 °C in a series of complicated weight losses until 885 °C. For **3**, the two steps of the weight loss of 5.14% between 30 and 268 °C correspond to the release of the two lattice water molecules (calculated, 5.34%). The residual framework decomposed beyond 450 °C in a series of complicated weight losses until 844 °C. For **4**, similar to **3**, the two steps of the weight loss of 5.46% between 30 and 280 °C correspond to the release of the two lattice water molecules (calculated, 5.35%). The residual framework decomposed beyond 428 °C in a series of complicated weight losses until 880 °C. For **5**, the first weight loss of 4.16% between 30 and 77 °C corresponds to the release of the lattice water molecules (calculated, 4.13%). The residual framework decomposed beyond 502 °C in a series of complicated weight losses and was still continuing when heating ended at 1000 °C. For **6**, the first weight loss of 82.21% between 80 and 184 °C corresponds to the release of the lattice and the coordinated water molecules (calculated, 82.66%). The residual framework decomposed beyond 409 °C in a series of complicated weight losses until 834 °C.

Conclusions

In this paper, we have presented the synthesis and crystal structures of six new MOFs from one to three dimensions, based on the 4,4'-H₂dbpt ligand. The structural diversities indicate that the 4,4'-H₂dbpt ligand could adopt different conformations according to the geometric requirements of metal ions and/or the introduction of auxiliary ligand owing to the different rotation angles of the four aromatic rings with respect to each other, deprotonation effort (4,4'-H₂dpbt, 4,4'-Hdpbt⁻, 4,4'-dpbt²⁻) and the flexing angles. As a result, five diverse and interesting architectures was obtained: **1** have a 2D (3, 6)-topology, with (4³)₃(4⁶.6⁶.8³)₂ Schläfli symbol. **2** have a 3D 8-connected topology with (3⁶.4¹⁸.5³.6) Schläfli symbol. **3** and **4** which are isostructural, both have a 2D 4-connected topology, with (4⁴.6²) Schläfli symbol. **5** have a complex 3D porous architecture with a 1D solvent-filled channel. **6** reveal a 1D helical chain extended along a quad screw axis. Accordingly, our present findings will further

enrich the crystal engineering strategy and offer the possibility of controlling the formation of the desired network structures.

Acknowledgment

We gratefully acknowledge the National Nature Science Foundation of China (Nos. 21101035, 21361003 and 21461003), Guangxi Natural Science Foundation of China (2012GXNSFBA053017, 2012GXNSFAA053035, and 2014GXNSFBA118056) and the Foundation of Key Laboratory for Chemistry and Molecular Engineering of Medicinal Resources.

References

- [1] (a) H. Furukawa, N. Ko, Y. B. Go, N. Aratani, S. B. Choi, E. Choi, A. O. Yazaydin, R. Q. Snurr, M. O'Keeffe, J. Kim and O. M. Yaghi, *Science*, 2010, **329**, 424- 428; (b) Y. Y. Liu, S. Couck, M. Vandichel, M. Grzywa, K. Leus, S. Biswas, D. Volkmer, J. Gascon, F. Kapteijn, J. F. M. Denayer, M. Waroquier, V. V. Speybroeck and P. V. D. Voort, *Inorg. Chem.*, 2013, **52**, 113- 120; (c) M. L. Foo, S. Horike, Y. Inubushi, S. Kitagawa, *Angew. Chem., Int. Ed.*, 2012, **51**, 6107- 6111; (d) J. H. Luo, H. W. Xu, Y. Liu, Y. S. Zhao, L. L. Daemen, C. Brown, T. V. Timofeeva, S. Q. Ma and H. C. Zhou, *J. Am. Chem. Soc.*, 2008, **130**, 9626- 9627; (e) L. Q. Ma, A. Jin, Z. G. Xie and W. B. Lin, *Angew. Chem. Int. Ed.*, 2009, **48**, 9905- 9908.
- [2] (a) A. Alberola, E. Coronado, J. R. Galán-Mascarós, C. Giménez-Saiz and C. J. Gómez-García, *J. Am. Chem. Soc.*, 2003, **125**, 10774- 10775; (b) H. Okawa, M. Sadakiyo, T. Yamada, M. Maesato, M. Ohba and H. Kitagawa, *J. Am. Chem. Soc.*, 2013, **135**, 2256- 2262; (c) U. Subbarao and S. C. Peter, *Cryst. Growth Des.*, 2013, **13**, 953- 959; (d) E. Coronado, J. R. Galán-Mascarós, C. J. Gómez-García and V. Laukhln, *Nature*, 2000, **408**, 447- 449.
- [3] (a) F. Nouar, J. Eckert, J. F. Eubank, P. Forster. M. Eddaoudi, *J. Am. Chem. Soc.*, 2009, **131**, 2864- 2870; (b) X. L. Zhao, X. Y. Wang, S. N. Wang, J. M. Dou, P. P. Cui, Z. Chen, D. Sun, X. P. Wang and D. F. Sun, *Cryst. Growth Des.*, 2012, **12**, 2736- 2739; (c) J. R. Choi, T. Tachikawa, M. Fujitsuka and T. Majima,

- Langmuir*, 2010, **26**, 10437- 10443; (d) C. A. Bauer, T. V. Timofeeva, T. B. Settersten, B. D. Patterson, V. H. Liu, B. A. Simmons and M. D. Allendorf, *J. Am. Chem. Soc.*, 2007, **129**, 7136- 7144; (e) K. A. White, D. A. Chengelis, K. A. Gogick, J. Stehman, N. L. Rosi and S. Petoud, *J. Am. Chem. Soc.*, 2009, **131**, 18069- 18071; (f) J. R. Li, Y. Tao, Q. Yu and X. H. Bu, *Chem. Commun.*, 2007, 1527- 1529; (g) B. Dey, R. Saha and P. Mukherjee, *Chem. Commun.*, 2013, **49**, 7064- 7066.
- [4] (a) Z. M. Wang, Y. J. Zhang, T. Liu, M. Kurmoo and S. Gao, *Adv. Funct. Mater.*, 2007, **17**, 1523-1536; (b) Z. R. Pan, H. G. Zheng, T. W. Wang, Y. Song, Y. Z. Li, Z. J. Guo and S. R. Batten, *Inorg. Chem.*, 2008, **47**, 9528-9536; (c) J. P. Zhao, Q. Yang, Z. Y. Liu, R. Zhao, B. W. Hu, M. Du, Z. Chang and X. H. Bu, *Chem. Commun.*, 2012, **48**, 6568-6570; (d) N. Yanai, W. Kaneko, K. Yoneda, M. Ohba and S. Kitagawa, *J. Am. Chem. Soc.*, 2007, **129**, 3496-3497; (e) P. Lama, J. Mrozinski and P. K. Bharadwaj, *Cryst. Growth Des.*, 2012, **12**, 3158-3168; (f) S. H. Cho, B. Ma, S. T. Nguyen, J. T. Hupp and T. E. Albrecht-Schmitt, *Chem. Commun.*, 2006, 2563-2565; (g) D. Pinkowicz, Z. Y. Li, P. Pietrzyk, M. Rams, *Cryst. Growth Des.* 2014, **14**, 4878– 4881.
- [5] (a) M. Y. Yoon, R. Srirambalaji and K. Kim, *Chem. Rev.*, 2012, **112**, 1196-1231; (b) D. W. Feng, Z. Y. Gu, J. R. Li, H. L. Jiang, Z. W. Wei, H. C. Zhou, *Angew. Chem., Int. Ed.*, 2012, **51**, 10307-10310; (c) J. M. Roberts, B. M. Fini, A. A. Sarjeant, O. K. Farha, J. T. Hupp and K. A. Scheidt, *J. Am. Chem. Soc.*, 2012, **134**, 3334-3337; (d) Z. L. Liao, G. D. Li, M. H. Bi, J. S. Chen, *Inorg. Chem.*, 2008, **47**, 4844-4853; (e) J. M. Zhang, A. V. Biradar, S. Pramanik, T. J. Emge, T. Asefa, J. Li, *Chem. Commun.*, 2012, **48**, 6541-6543; (f) L. Q. Ma, C. Abney, W. B. Lin, *Chem. Soc. Rev.*, 2009, **38**, 1248-1256.
- [6] (a) O. D. Friedrichs, M. O’Keeffe and O. M. Yaghi, *Acta Crystallogr., Sect. A: Found. Crystallogr.*, 2003, **59**, 22; (b) O. D. Friedrichs, M. O’Keeffe and O. M. Yaghi, *Acta Crystallogr., Sect. A: Found. Crystallogr.*, 2003, **59**, 515; (c) L. Pan, D. H. Olson, L. R. Ciemmolonski, R. Heddy and J. Li, *Angew. Chem., Int. Ed.*, 2006, **45**, 616-619; (d) A. Y. Robin and K. M. Fromm, *Coord. Chem. Rev.*, 2006,

- 250**, 2127-2157; (e) C. Pan, J. P. Nan, X. L. Dong, X. M. Ren and W. Q. Jin, *J. Am. Chem. Soc.*, 2011, **133**, 12330-12333; (g) X. Z. Song, S. Y. Song, C. Qin, S. Q. Su, S. N. Zhao, M. Zhu, Z. M. Hao and H. J. Zhang, *Cryst. Growth Des.*, 2012, **12**, 253-263.
- [7] (a) Y.-L. Wang, D.-Q. Yuan, W.-H. Bi, X. Li, X.-J. Li, F. Li, R. Cao, *Cryst. Growth Des.*, 2005, **5**, 1849-1855; (b) Y.-B. Lu, M.-S. Wang, W.-W. Zhou, G. Xu, G.-C. Guo, J.-S. Huang, *Inorg. Chem.*, 2008, **47**, 8935-8942; (c) O. Fabelo, J. Pasan, F. Lloret, M. Julve, C.R. Perez, *Inorg. Chem.*, 2008 **47** 3568-3576.
- [8] (a) W.-G. Lu, L. Jiang, X.-L. Feng, T.-B. Lu, *Cryst. Growth Des.*, 2008, **8**, 986-994; (b) A.-X. Tian, J. Ying, J. Peng, J.-Q. Sha, H.-J. Pang, P.-P. Zhang, Y. Chen, M. Zhu, Z.-M. Su, *Inorg. Chem.*, 2009, **48**, 100-110.
- [9] (a) Y. Wang, X.-Q. Zhao, W. Shi, P. Cheng, D.-Z. Liao, S.-P. Yan, *Cryst. Growth Des.*, 2009, **9**, 2137-2145; (b) J. Park, S. Hong, D. Moon, M. Park, K. Lee, S. Kang, Y. Zou, R. P. John, G. H. Kim, M. S. Lah, *Inorg. Chem.*, 2007, **46**, 10208-10213; (c) C.-H. Li, K.-L. Huang, Y.-N. Chi, X. Liu, Z.-G. Han, L. Shen, C.-W. Hu, *Inorg. Chem.*, 2009, **48**, 2010-2017.
- [10] (a) L. S. Long, *CrystEngComm*, 2010, **12**, 1354-1365; (b) M. Tsaramyrsi, M. Kaliva, A. Salifoglou, C. P. Raptopoulou, A. Terzis, V. Tangoulis and J. Giapintzakis, *Inorg. Chem.*, 2001, **40**, 5772-5779; (c) S. Faulkner, B. P. Burton-Pye, *Chem. Commun.*, 2005, 259-261; (d) L. N. Zhang, S. T. Lu, C. Zhang, C. X. Du, H. W. Hou, *CrystEngComm*, 2015, **17**, 846-855.
- [11] (a) Y. Tao, J.-R. Li, Q. Yu, W.-C. Song, X.-L. Tong, X.-H. Bu, *CrystEngComm.*, 2008, **10**, 699-705. (b) B. Zheng, H. Dong, J. Bai, Y. Li, S. Li, M. Scheer, *J. Am. Chem. Soc.*, 2008, **130**, 7778-7779.
- [12] (a) H. Furukawa, Y. B. Go, N. Ko, Y. K. Park, F. J. Uribe-Romo, J. Kim, M. O'Keeffe and O. M. Yaghi, *Inorg. Chem.*, 2011, **50**, 9147-9152; (b) J. J. Gassensmith, H. Furukawa, R. A. Smaldone, R. S. Forgan, Y. Y. Botros, O. M. Yaghi, J. F. Stoddart, *J. Am. Chem. Soc.*, 2011, **133**, 15312-15315; (c) K. M. Choi, H. J. Jeon, J. K. Kang, O. M. Yaghi, *J. Am. Chem. Soc.*, 2011, **133**, 11920-11923; (d) A. Phan, A. U. Czaja, F. Ga'ndara, C. B. Knobler and O. M.

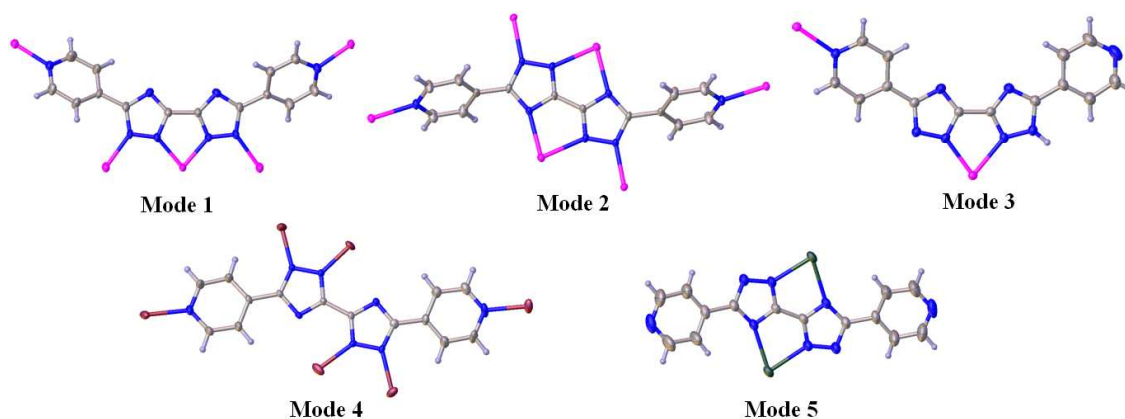
- Yaghi, *Inorg. Chem.*, 2011, **50**, 7388-7390; (e) J. Song, Z. Luo, D. K. Britt, H. Furukawa, O. M. Yaghi, K. I. Hardcastle, C. L. Hill, *J. Am. Chem. Soc.*, 2011, **133**, 16839-16846.
- [13] (a) R. B. Getman, J. H. Miller, K. Wang and R. Q. Snurr, *J. Phys. Chem. C*, 2011, **115**, 2066-2075; (b) X. Y. Bao, R. Q. Snurr, L. J. Broadbelt, *Langmuir*, 2009, **25**, 10730-10736.
- [14] (a) X. M. Chen and G. F. Liu, *Chem.–Eur. J.*, 2002, **8**, 4811-4817; (b) J. P. Zhang, Y. Y. Lin, X. C. Huang and X. M. Chen, *J. Am. Chem. Soc.*, 2005, **127**, 5495-5506; (c) L. Cheng, W. X. Zhang, B. H. Ye, J. B. Lin and X. M. Chen, *Inorg. Chem.*, 2007, **46**, 1135-1143; (d) J. P. Zhang, X. L. Qi, Z. J. Liu, A. X. Zhu, Y. Chen, J. Wang and X. M. Chen, *Cryst. Growth Des.*, 2011, **11**, 796-802; (e) J. B. Lin, J. P. Zhang, W. X. Zhang, W. Xue, D. X. Xue and X. M. Chen, *Inorg. Chem.*, 2009, **48**, 6652-6660.
- [15] (a) C. P. Li, J. M. Wu and M. Du, *Inorg. Chem.*, 2011, **50**, 9284-9289; (b) L.- F. Ma, C.- P. Li, L.- Y. Wang, M. Du, *Cryst. Growth Des.*, 2010, **10**, 2641-2649; (c) C.- P. Li, Q. Yu, J. Chen, M. Du, *Cryst. Growth Des.*, 2010, **10**, 2650-2660; (d) M. Du, Q. Wang, C.- P. Li, X.- J. Zhao, J. Ribas, *Cryst. Growth Des.*, 2010, **10**, 3285-3289.
- [16] (a) Z. Yan, Z. P. Ni, F. S. Guo, J. Y. Li, Y. C. Chen, J. L. Liu, W. Q. Lin, D. Aravena, E. Ruiz, M. L. Tong, *Inorg. Chem.*, 2014, **53**, 201-208; (b) Z. Yan, J. Y. Li, T. Liu, Z. P. Ni, Y. C. Chen, F. S. Guo, M. L. Tong, *Inorg. Chem.*, 2014, **53**, 8129-8135.
- [17] (a) X. T. Zhang, L. M. Fan, Z. Sun, W. Zhang, D. C. Li, J. M. Dou, L. Han, *Cryst. Growth Des.*, 2013, **13**, 792-803; (b) L. M. Fan, X. T. Zhang, Z. Sun, W. Zhang, Y. S. Ding, W. L. Fan, L. M. Sun, X. Zhao, H. Lei, *Cryst. Growth Des.*, 2013, **13**, 2462-2475.
- [18] (a) F.-P. Huang, J.-L. Tian, W. Gu, X. Liu, S.-P. Yan, D.-Z. Liao, P. Cheng, *Cryst. Growth Des.*, 2010, **10**, 1145-1154; (b) F.-P. Huang, H.-Y. Li, Q. Yu, H.-D. Bian, J.-L. Tian, S.-P. Yan, D.-Z. Liao, P. Cheng, *CrystEngComm.*, 2012, **14**, 4756-4766; (c) F.-P. Huang, J.-L. Tian, D.-D. Li, G.-J. Chen, W. Gu, S.-P. Yan, X.

- Liu, D.-Z. Liao, P. Cheng, *Inorg. Chem.*, 2010, **49**, 2525-2529; (d) F.-P. Huang, Q. Zhang, Q. Yu, H.-D. Bian, H. Liang, S.-P. Yan, D.-Z. Liao, P. Cheng, *Cryst. Growth Des.*, 2012, **12** 1890-1898; (e) F. P. Huang, P. F. Yao, Q. Yu, D. Yao, H. D. Bian, H. Y. Li, J. L. Tian, S. P. Yan, *Inorg. Chem. Commun.*, 2013, **31** 18-22; (f) F. P. Huang, Z. M. Yang, P. F. Yao, Q. Yu, J. L. Tian, H. D. Bian, S. P. Yan, D. Z. Liao, P. Cheng, *CrystEngComm*, 2013, **15**, 2657-2668; (g) F. P. Huang, P. F. Yao, W. Luo, H. Y. Li, Q. Yu, H. D. Bian, S. P. Yan, *RSC Adv.*, 2014, **4**, 43641-43652; (e) F.-P. Huang, J.-L. Tian, D.-D. Li, G.-J. Chen, W. Gu, S.-P. Yan, X. Liu, D.-Z. Liao, P. Cheng, *CrystEngComm*, 2010, **12**, 395-400.
- [19] (a) Z. Q. Xu, Q. Wang, H. J. Li, W. Meng, Y. Han, H. W. Hou, Y. T. Fan, *Chem. Commun.*, 2012, **48**, 5736-5738; (b) Z. Q. Xu, W. Meng, H. J. Li, H. W. Hou, Y. T. Fan, *Inorg. Chem.*, 2014, **53**, 3260-3262; (c) Z. Q. Xu, H. J. Li, A. R. Li, W. Meng, H. W. Hou, Y. T. Fan, *Inorg. Chem. Commun.*, 2013, **36**, 126-129.
- [20] (a) W. W. Dong, D. S. Li, J. Zhao, L. F. Ma, Y. P. Wu, Y. P. Duan, *CrystEngComm*, 2013, **15**, 5412-5416; (b) W. W. Dong, D. S. Li, J. Zhao, Y. P. Wu, Y. Y. Wang, *Inorg. Chem. Commun.*, 2012, **21** 53-56.
- [21] M. T. Li, J. Q. Sha, X. M. Zong, J. W. Sun, P. F. Yan, L. Li, X. N. Yang, *Cryst. Growth Des.*, 2014, **14**, 2794-2802.
- [22] Y. H. Zhou, W. Q. Wan, D. L. Sun, J. Tao, L. Zhang, X. W. Wei, *Z. Anorg. Allg. Chem.*, 2014, **640**, (1), 249-253.
- [23] (a) J. P. Zhang, Y. B. Zhang, J. B. Lin, X. M. Chen, *Chem. Rev.*, 2012, **112**, 1001; (b) J. G. Haasnoot, *Coord. Chem. Rev.*, 2000, **200–202**, 131-185; (c) T.-F. Liu, J. Lü, C. B. Tian, M. N. Cao, Z. J. Lin, R. Cao, *Inorg. Chem.* 2011, **50**, 2264–2271.
- [24] N. N. Vyatsheslav, V. Z. Nikolay, Z. V. Sergey, *ARKIVOC*, 2005, 118.
- [25] SAINT Software Reference Manual; Bruker AXS: Madison, WI, 1998.
- [26] G. M. Sheldrick, Phase Annealing in SHELX-90: Direct Methods for Larger Structures. *Acta Crystallogr.* 1990, **A46**, 467-473.
- [27] G. M. Sheldrick, SHELXS-97, Program for X-ray Crystal Structure Solution; University of Göttingen: Göttingen, Germany, 1997.
- [28] (a) M. O'Keeffe and O. M. Yaghi, Reticular Chemistry Structure Resource,

- Arizona State University, Tempe, AZ, **2005**, <http://www.okeeffews1.1a.asu.edu/rcsr/home.htm>; (b) V. A. Blatov, Multipurpose crystallochemical analysis with the program package TOPOS, IUCr CompComm Newsletter, 2006, **vol. 7**, p. 4; (c) V. A. Blatov, A. P. Shevchenko, V. N. Serezhkin, *J. Appl. Crystallogr.*, 2000, **33**, 1193; (d) A. F. Wells, Three-Dimensional Nets and Polyhedra, *Wiley Interscience, New York*, 1977.
- [29] (a) L.-H. Jia, R.-Y. Li, Z.-M. Duan, S.-D. Jiang, B.-W. Wang, Z.-M. Wang, S. Gao, *Inorg. Chem.*, 2011, **50**, 144-254; (b) N. Marino, O. F. Ikotun, M. Julve, F. Lloret, J. Cano, R. P. Doyle, *Inorg. Chem.*, 2011, **50**, 378-389; (c) T. D. Keene, I. Zimmermann, A. Neels, O. Sereda, J. Hauser, M. Bonin, M. B. Hursthouse, D. J. Price, S. Decurtins, *Dalton Trans.*, 2010, 4937-4950; (d) L.-Q. Wei, B.-W. Li, S. Hu, M.-H. Zeng, *CrystEngComm.*, 2011, **13**, 510-516; (e) S.-Q. Zang, X.-M. Ren, Y. Su, Y. Song, W.-J. Tong, Z.-P. Ni, H.-H. Zhao, S. Gao, Q.-J. Meng, *Inorg. Chem.*, 2009, **48**, 9623-9630.
- [30] (a) X.-Y. Wang, H.-Y. Wei, Z.-M. Wang, Z.-D. Chen, S. Gao, *Inorg. Chem.*, 2005, **44**, 572-583; (b) E. K. Brechin, O. Cador, A. Caneschi, C. Cadiou, S. G. Harris, S. Parsons, M. Vooni, R. E. P. Winpenny, *Chem. Commun.*, 2002, 1860-1861; (c) A. Escuer, J. Cano, M. A. S. Goher, Y. Journaux, F. Lloret, F. A. Mautner, R. Vicente, *Inorg. Chem.* 2000, **39**, 4688-4695; (d) X.-N. Cheng, W. Xue, W.-X. Zhang, X.-M. Chen, *Chem. Mater.* 2008, **20**, 5345-5350; (e) F.-P. Huang, J.-L. Tian, D.-D. Li, G.-J. Chen, W. Gu, S.-P. Yan, X. Liu, D.-Z. Liao, P. Cheng, *Inorg. Chem.* 2010, **49**, 2525-2529.
- [31] (a) J. A. Mydosh, *Spin Glasses: An Experimental Introduction*, Taylor & Francis, London, 1993; (b) X.-N. Cheng, W. Xue, J.-B. Lina, X.-M. Chen, *Chem. Commun.*, 2010, 246-248.
- [32] R. Ruamps, R. Maurice, L. Batchelor, M. Boggio-Pasqua, R. Guillot, A. L. Barra, J. J. Liu, E. E. Bendeif, S. Pillet, S. Hill, T. Mallah, N. Guihéry, *J. Am. Chem. Soc.*, 2013, **135**, 3017-3026.

Table 1 Crystal data and structure refinement for **1– 6**.

Complex	1	2	3	4	5	6
Empirical formula	C ₄₀ H ₄₈ Cl ₈ Co ₅ N ₁₈	C _{30.5} H ₁₈ Co ₃ N ₈ O _{8.5}	C ₂₈ H ₂₂ CoN ₁₆ O ₂	C ₂₈ H ₂₂ NiN ₁₆ O ₂	C ₁₄ H ₁₀ Cu ₂ N ₈ O	C ₁₄ H ₁₆ MnN ₈ O ₄
Formula weight	1359.20	809.32	673.55	673.33	433.36	415.29
Crystal system	Triclinic	Triclinic	Monoclinic	Monoclinic	Orthorhombic	Tetragonal
Space group	<i>P</i> -1	<i>P</i> -1	<i>P</i> 2 ₁ / <i>n</i>	<i>P</i> 2 ₁ / <i>n</i>	<i>Pbcn</i>	<i>I</i> 4 ₁ / <i>acd</i>
<i>a</i> (Å)	11.5936 (6)	9.2529 (12)	9.2567 (10)	9.1787 (10)	14.6978 (14)	19.1314 (3)
<i>b</i> (Å)	11.9201 (7)	10.6355 (11)	15.269 (4)	15.2181 (11)	19.3933 (17)	19.1314 (3)
<i>c</i> (Å)	12.1223 (6)	11.0493 (13)	10.2578 (3)	10.3355 (8)	10.3560 (9)	20.6667 (3)
α (°)	63.593 (5)	63.622 (11)	90	90	90	90
β (°)	88.025 (4)	86.489 (10)	96.720 (5)	96.657 (8)	90	90
γ (°)	67.331 (5)	74.907 (10)	90	90	90	90
Volume (Å ³)	1365.40 (12)	938.68 (19)	1439.9 (4)	1433.9 (2)	2951.9 (5)	7564.2 (2)
<i>Z</i>	1	1	2	2	8	16
Calculated density(Mg/m ³)	1.651	1.432	1.554	1.559	1.941	1.459
Goodness-of-fit on <i>F</i> ²	1.040	1.171	1.040	1.029	1.033	1.079
Independent reflections	5578	3840	2938	2922	3018	1933
<i>R</i> _{int}	0.0712	0.0249	0.0247	0.0841	0.0521	0.0313
<i>R</i> ₁ [<i>I</i> > 2σ(<i>I</i>)]	0.0652	0.0596	0.0391	0.0530	0.0538	0.0397
w <i>R</i> ₂ (all data)	0.1433	0.1933	0.0963	0.1073	0.1390	0.1180



Scheme 1 The versatile coordination modes of 4,4'-H₂dbpt used in this work.

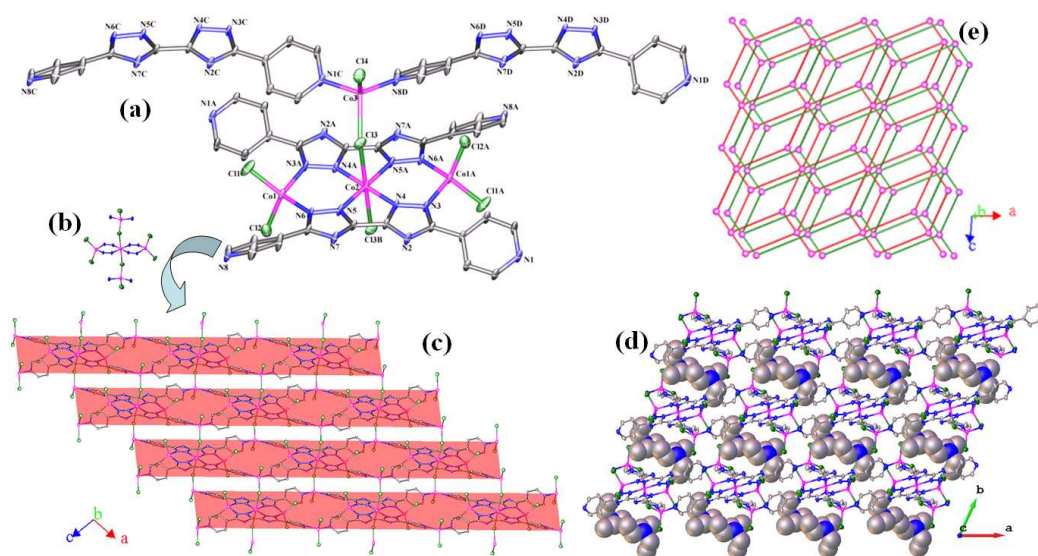


Fig. 1 (a) The coordination environment of the Co(II) atoms (Symmetry codes: A: $x, y, z+1$; B: $x+1, y, z$; C: $-x+1, -y+1, -z+1$; D: $x, y, z-1$); (b) The Co₅ unit; (c) View of the 2D ladder network; (d) The 3D extended structure; (e) the schematic description for the 2D architecture with $(4^3)_3(4^6.6^6.8^3)_2$ symbol.

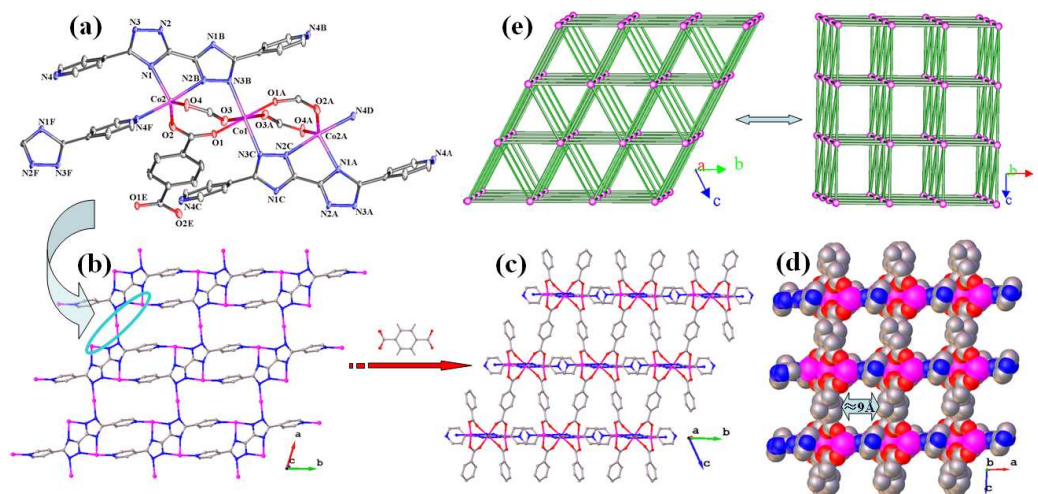


Fig. 2 (a) The coordination environment of the Co(II) atoms (Symmetry codes: A: $-x+1, -y+1, -z+1$; B: $-x, -y+1, -z+1$; C: $x+1, y, z$; D: $-x, -y, -z+1$; E: $x-1, y, z$; F: $-x+1, -y, -z+2$); (b) View of the 2D network connected by the 4,4'- dbpt ligand; (c) View of the 3D network along the a axis; (d) The 3D network with parallel channels along the b axis; (e) the schematic description for the 3D architecture with $(3^6.4^{18}.5^3.6)$ symbol.

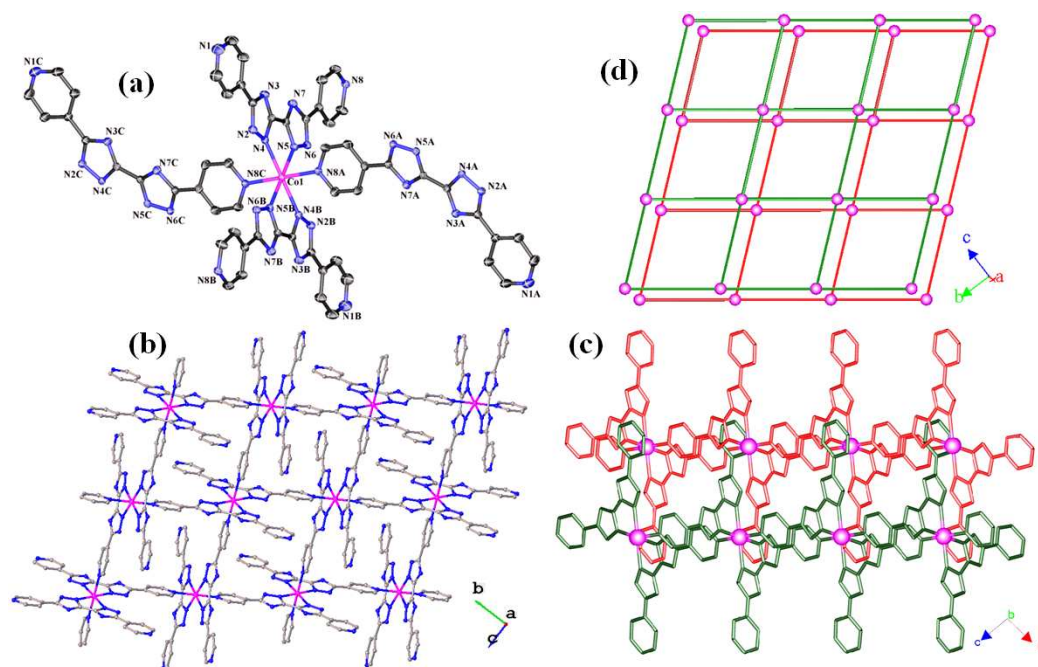


Fig. 3 (a) The coordination environment of the M(II) atoms (Symmetry codes: A: $-x+1, -y, -z+2$; B: $x+1/2, -y-1/2, z-1/2$; C: $-x+1/2, y+1/2, -z+5/2$); (b) View of the 2D network connected by the 4,4'- Hdbpt ligand; (c) The 3D extended structure; (d) the schematic description for the 3D architecture with $(4^4.6^2)$ symbol.

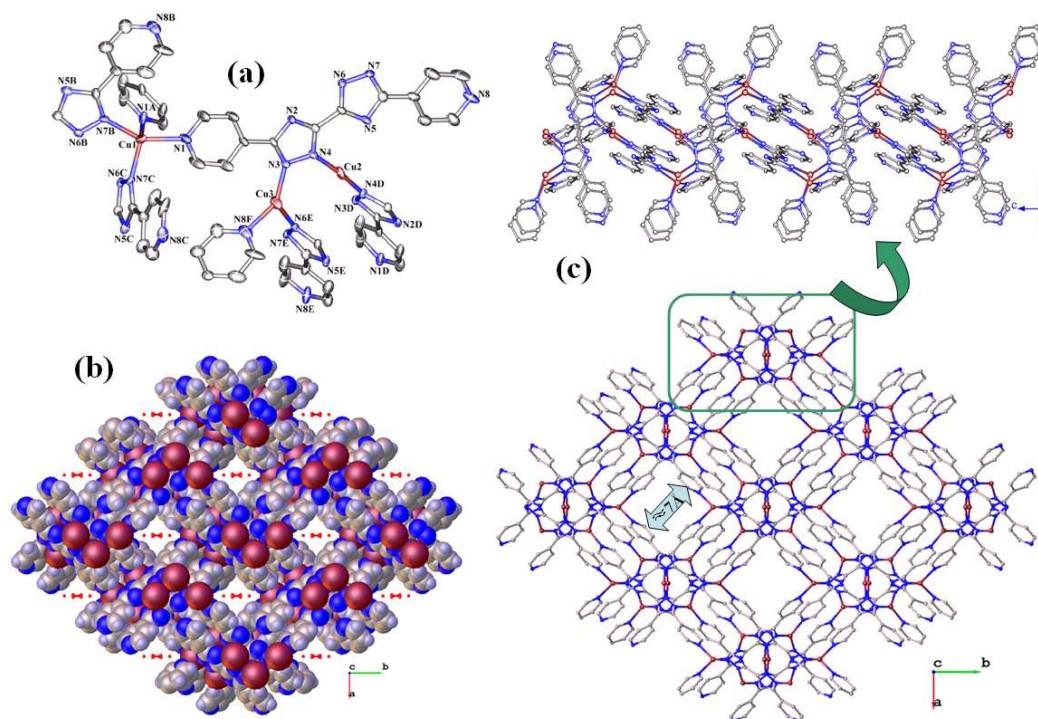


Fig. 4 (a) The coordination environment of the Cu(I) atoms (Symmetry codes: A: $-x$, y , $-z+1/2$; B: $-x+1/2$, $y-1/2$, z ; C: $x-1/2$, $y-1/2$, $-z+1/2$; D: $-x+1$, y , $-z+3/2$; E: x , $-y+1$, $z+1/2$; F: $x-1/2$, $y-1/2$, $-z+3/2$.); (b) The space-filling plot of the 3D network connected by the 4,4'-dbpt ligand; (c) View of the 3D network connected by the 4,4'-dbpt ligand.

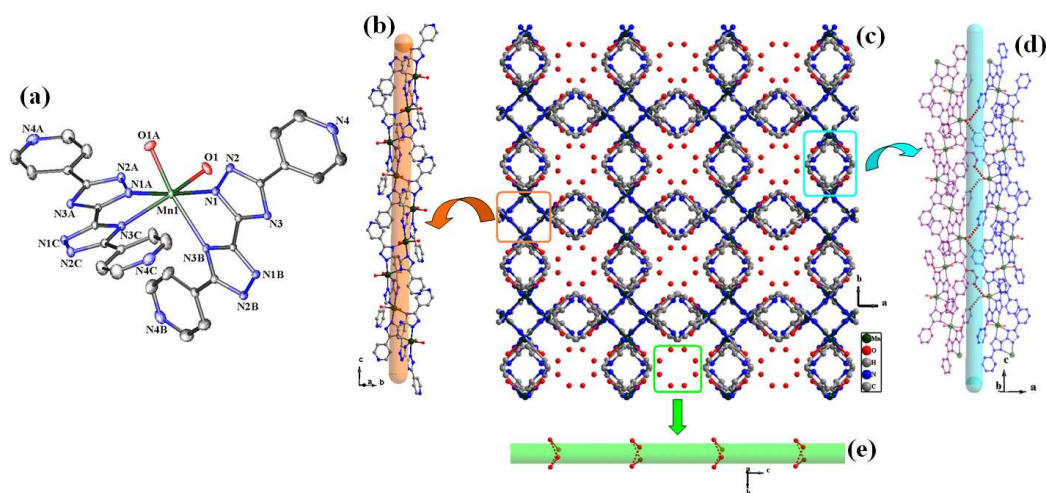


Fig. 5 (a) The coordination environment of the Mn(II) atoms (Symmetry codes: A: $-x+1/2$, y , $-z$; B: $-y+1/4$, $-x+1/4$, $-z+1/4$; C: $y+1/4$, $-x+1/4$, $z-1/4$); (b) View of the

helical chain extended along the c axis; (c) View of the 3D extended structure along the c axis; (d) The connection type of the H-bond between the adjacent helical chains; (e) arrangement of lattice water molecules filling in the gaps of the neighbor chains.

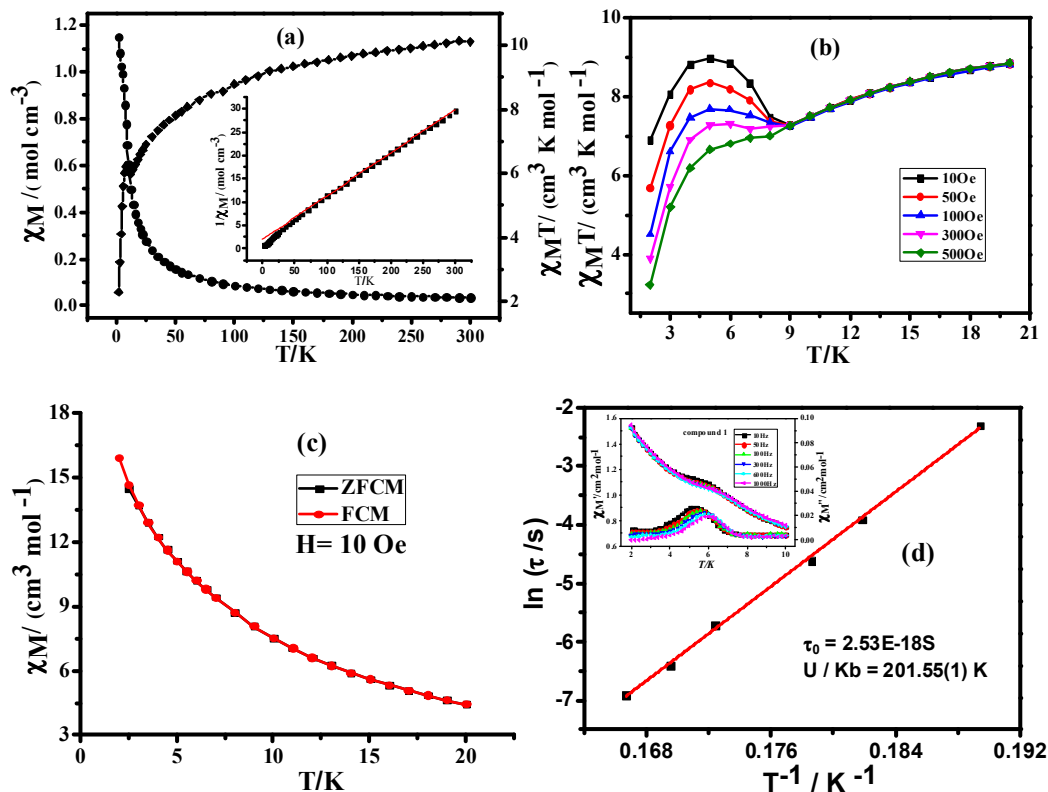
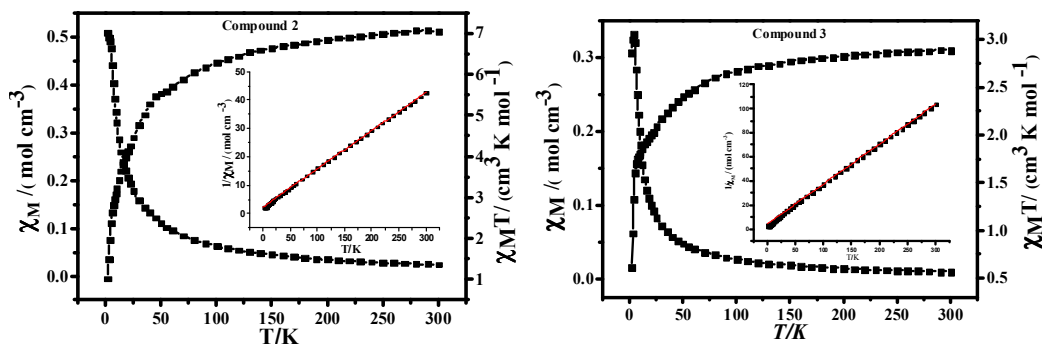


Fig. 6 (a) Plots of $\chi_M T$ vs T and χ_M^{-1} vs T (inset) for **1**; (b) FC magnetization of them in different field; (c) Plots of zero-field cooled magnetization (ZFC) and field-cooled magnetization (FC) and in a field of 10 Oe for **1** using a SQUID; (d) Arrhenius plot for **1** fitted by Arrhenius law $\tau = \tau_0 \exp(-\Delta E/k_B T)$, Inset: the zero-field ac magnetic susceptibilities for **1**.



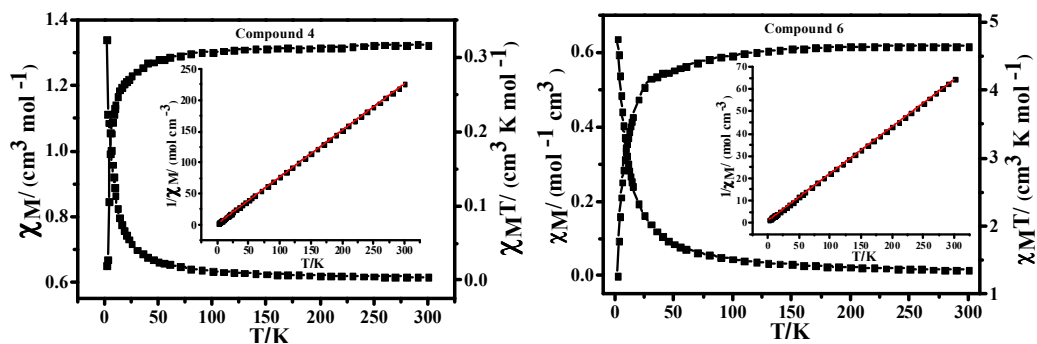


Fig. 7 Plots of $\chi_M T$ vs T and χ_M^{-1} vs T (inset) for 2- 4 and 6.

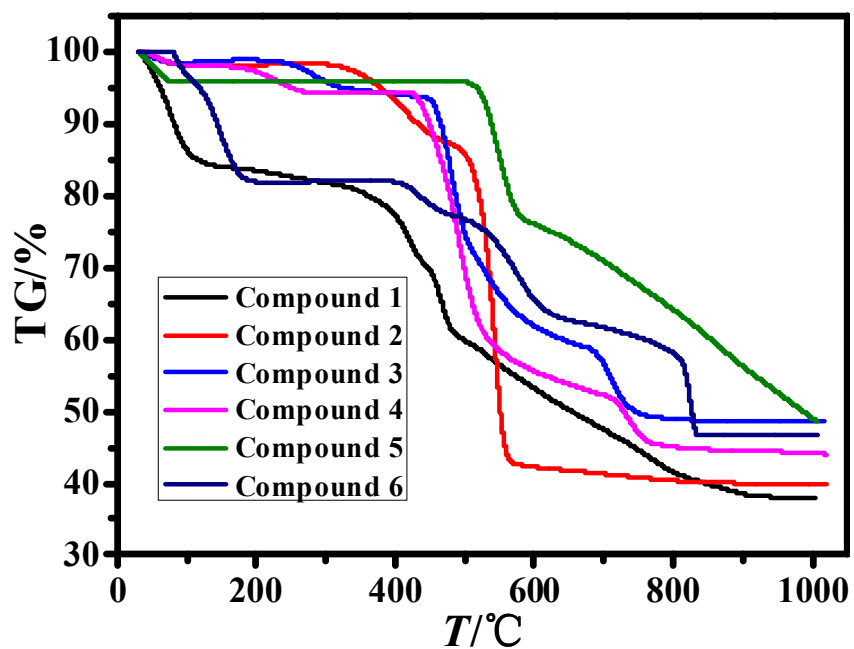


Fig. 8 TG curves for Complexes 1– 6.